

# Interaction between two horizontal axis tidal turbines in model scale - experiment and simulation

Simon Joßberger, Christa Stadler, Ulf Barkmann, Nicholas Kaufmann and Stefan Riedelbauch

**Abstract**—Up to 6 Schottel Instream Turbines (SIT250) can be mounted on the tidal platform PLAT-I developed by Sustainable Marine Energy. Due to the close proximity of the turbines interactions can occur between them. Two horizontal axis tidal turbines in model scale are investigated experimentally and numerically to analyze these interactions. Experimental data were measured in a towing tank and consist of integral values for torque, thrust and rotational speed. Both a steady state and an unsteady three-dimensional Reynolds Averaged Navier Stokes (RANS) approach are utilized for simulating the turbine flow field. The first part of the paper compares simulation results of a single turbine at different tip speed ratios with measurements to validate the numerical approach and its employed models. The second part analyses the interaction between two turbines. The axial distance in main flow direction between the turbines is half the rotor diameter. The radial distance measured between the hubs of the turbines is varied in steps of 0.2 between 0.0 and 2.0 times the rotor diameter in the experiment and between 0.0 and 1.4 in the simulations. Measurements were conducted for tip speed ratios of 3, 4 and 5. In the simulations the tip speed ratio was fixed at 4. The used simulation domain replicates the actual width and height of the towing tank and a sufficient length up- and downstream of the turbines. The water surface is modeled with a free slip wall. Both thrust and torque are compared between simulation results and experimental data. Furthermore, a detailed analysis of the results and flow field in the numerical simulations is presented and the interaction between the turbines is discussed.

**Index Terms**—Tidal turbine, Interaction, Model scale, CFD, Simulation, Experiment.

## I. INTRODUCTION

Manuscript received December 16th, 2021, published 29 September 2022. This is an open access article distributed under the terms of the Creative Commons Attribution 4.0 licence (CC BY <http://creativecommons.org/licenses/by/4.0/>). Unrestricted use (including commercial), distribution and reproduction is permitted provided that credit is given to the original author(s) of the work, including a URI or hyperlink to the work, this public license and a copyright notice. This article has been subject to single-blind peer review by a minimum of two reviewers.

This work was supported in part by the Federal Ministry for Economic Affairs and Energy of Germany (BMWi) in the project OsT under grant 03EE4001C.

S. Joßberger, C. Stadler and S. Riedelbauch are with Institute of Fluid Mechanics and Hydraulic Machinery, University of Stuttgart, Pfaffenwaldring 10, 70569 Stuttgart, Germany (e-mail: simon.jossberger@ihs.uni-stuttgart.de).

U. Barkman was with Schiffbau-Versuchsanstalt Potsdam GmbH, Marquardtter Chaussee 100, 14469 Potsdam, Germany and is now an independent developer and consultant (e-mail: ulf.barkmann@gmx.de).

N. Kaufmann is with Schottel Hydro GmbH, Mainzer Str. 99, 56322 Spay, Germany (e-mail: nkaufmann@schottel.de).

Digital Object Identifier: <https://doi.org/10.36688/imej.5.173-182>

**T**HE tidal platform PLAT-I developed by Sustainable Marine Energy can support up to 6 Schottel Instream Turbines SIT250 in one row with no axial offset. The limited space on the platform leads to small lateral distances between the turbines. Details on the platform can be found, for example, in Starzmann et. al [1], [2] and Kaufmann et. al [3]

Prior investigations in the literature focus on experimental and numerical studies of turbine array configurations, where the turbines are arranged in multiple rows with no overlap and the axial distance is at least 4 rotor diameters.

Myers and Bahaj [4] conducted experiments with porous actuator disks instead of actual turbines to study the wake and thrust of up to 3 disks in two rows. Stallard et. al [5] performed measurements on an array of up to two rows with a maximum of 5 turbines each. The minimum radial distance between the turbines was 1.5 diameter and the minimum axial distance 4 diameters. Mycek et. al [6], [7] measured two radially aligned turbines with an axial distance between 2 and 12 diameters. Malki et. al [8] simulated array configurations of up to 14 turbines with an combined Blade Element Method (BEM) for the turbines and a 3D-CFD approach for the surrounding flow. The axial distance ranged between 5 and 30 diameters and the radial distance between 1.5 and 5.0 diameters. Hunter et. al [9] performed simulations with a combined RANS and Actuator Disk approach to individually tune the operating state of up to 8 turbines with a fixed radial distance of 1.25 diameters in two rows. Olczak et. al [10] conducted RANS-BEM simulations and measurements of different arrays of up to 12 turbines in 3 rows with a minimum radial distance of 1.5 diameters and a minimum axial distance of 4 diameters.

In the present paper the interaction of two turbines in very close proximity with an axial distance of 0.5 diameter and a variable radial distance between 0.0 and 2.0 diameters is investigated. In the first part simulation results of a single turbine at different tip speed ratios are compared with measurements to validate the numerical approach and its employed models. In the second part the results of measurements and simulations for the double turbine configuration are analysed.

## II. GEOMETRY

The turbines for both the single and double turbine configuration are Schottel Instream Turbines (SIT250)

TABLE I  
NOMENCLATURE

Symbol	Quantity	Unit
$D_s$	Diameter of turbine in single turbine configuration	m
$D_d$	Diameter of turbine in double turbine configuration	m
$A = \frac{\pi}{4} D^2$	Swept rotor area	m <sup>2</sup>
$r$	Radial distance between turbines	m
$a$	Axial distance between turbines	m
$\omega$	Rotational speed	1/s
$u_\infty$	Freestream velocity	m/s
$\lambda = \frac{\omega 0.5D}{u_\infty}$	Tip speed ratio	[-]
$\Phi$	Phase angle	°
$y^+$	Dimensionless wall distance	[-]
$\Delta t$	Time step size	s
$\rho$	Density	kg/m <sup>3</sup>
$\mu$	Dynamic viscosity	Pa·s
$c_{70}$	Chord length at 70% radius	m
$w_{70} = \frac{\sqrt{u_\infty^2 + (0.7\lambda u_\infty)^2}}{\mu}$	Relative velocity at 70% radius	m/s
$Re_{70} = \frac{\rho c_{70} w_{70}}{\mu}$	Reynolds number at 70% radius	[-]
$Re_{crit}$	Critical Reynolds number	[-]
$T$	Thrust	N
$P$	Power	W
$C_T = \frac{T}{0.5\rho A u_\infty^2}$	Thrust coefficient	[-]
$C_P = \frac{P}{0.5\rho A u_\infty^3}$	Power coefficient	[-]
$C_Q = \frac{C_P}{\lambda}$	Torque coefficient	[-]

in model scale. The SIT250 is a horizontal axis tidal turbine with 3 blades. Details on the turbine can be found in Kaufmann et. al [3], [11]. The diameter of the turbine is  $D_s = 500$  mm in the single turbine configuration and  $D_d = 235.3$  mm for both turbines in the double turbine configuration. Fig. 1 shows the assembly of the double turbine configuration. The turbines are mounted on two dynamometers of different size. The immersion depth of the upstream turbine in cyan is fixed at one diameter  $D_d$  measured from the axis of rotation. The radial distance between the two turbines  $r$  is varied in steps of  $0.2 D_d$  between  $0.0 D_d$  and  $2.0 D_d$  in the experiment and  $0.0 D_d$  and  $1.4 D_d$  in the simulations. The axial distance is fixed at half a diameter  $a/D_d = 0.5$ . There is no offset in lateral direction. Looking in streamwise direction the upstream turbine is rotating in counter clock wise direction and the downstream turbine in clock wise direction.

Similar to the downstream turbine in magenta in Fig. 1 the shown push configuration with the same dynamometer is used for the single turbine. The immersion depth is one diameter  $D_s$  measured from the axis of rotation.

### III. EXPERIMENTAL SETUP

All measurements were performed in the towing tank of the Schiffbau-Versuchsanstalt Potsdam. The width, height and length of the towing tank are 9.0 m, 4.5 m and 280.0 m respectively. In the double turbine configuration the turbines are mounted on the

free-running dynamometers H29 (upstream) and H39 (downstream). The single turbine is mounted on the dynamometer H39. According to the recommendations of the International Towing Tank Conference (ITTC), the measured values for thrust and torque are corrected using the values obtained for a dummy hub of the same mass as the investigated model turbine for both dynamometers [12].

Measurements of the double turbine configuration are performed for a fixed towing velocity of  $u_\infty = 1.5$  m/s and three tip speed ratios  $\lambda = [3.0, 4.0, 5.0]$ . The single turbine is measured with a towing velocity of  $u_\infty = 3.0$  m/s and different  $\lambda$  between about 0 and 10.

## IV. NUMERICAL SETUP AND MESH

### A. Numerical setup

The simulations are conducted with ANSYS CFX in version 19.2 for the single turbine and version 2020 R2 (20.2) for the double turbine configuration. The computational domain and the boundary conditions are shown in Fig. 2. The domain utilizes the actual width and height of 9.0 m ( $\approx 40D_d$ ) and 4.5 m ( $\approx 20D_d$ ) of the towing tank. A length of about 12.0 m upstream ( $\approx 50D_d$ ) and 18.0 m ( $\approx 75D_d$ ) downstream the turbines is modelled. Whereas in reality the turbines are moving through the static towing tank, in the simulation the state of motion is reversed. At the inlet a constant uniform velocity of  $u_\infty = 3$  m/s and  $u_\infty = 1.5$  m/s is set for the single and double turbine configuration, respectively. Bottom and side walls are set as moving walls with the same velocity specified at the inlet. At the outlet a constant static pressure of 0 Pa is set. The water surface is modelled as a frictionless free slip wall. Water is used as an incompressible fluid at a constant temperature of 20 °C with a density of  $\rho = 977$  kg/m<sup>3</sup> and dynamic viscosity of  $\mu = 8.89 \cdot 10^{-4}$  Pa·s. Turbulence is modelled with the k- $\omega$  SST model. As turbulence properties at the inlet an eddy length scale of 1 mm and a turbulent intensity of 5 % is specified. Automatic wall treatment is used for the boundary layer. Depending on the dimensionless wall distance  $y^+$  wall functions or a direct calculation with a Low-Re approach of the viscous sublayer are used.

Multiple frames of reference are used to simulate the rotating turbine domains and the stationary far field domain. The domains are connected with a mixing plane interface in the steady state simulations and a full 360° transient rotor stator interface in the unsteady simulations. The mixing plane interface performs an averaging of the fluxes on circumferential bands and steady state solutions are calculated in each domain. Due to the averaging process the relative position of the turbines is not important. This type of interface can account for time average interaction effects but is not capable to capture unsteady phenomena. The transient rotor stator interface simulates the relative motion between the different domains. Hence, it is capable to account for all interaction effects.

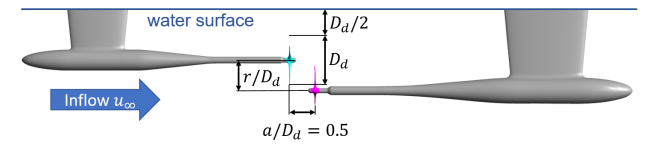


Fig. 1. Geometry of double turbine configuration. Radial distance in shown example  $r/D_d = 0.6$ .

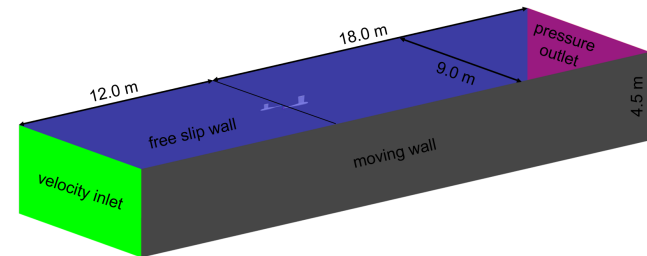


Fig. 2. Computational domain and boundary conditions for simulations.

The tip speed ratio  $\lambda$  is fixed to 4 for the double turbine configuration and varied in the interval  $\lambda \in [3.0, 4.0, 5.0, 6.5, 8.0]$  for the single turbine configuration. ANSYS CFX uses a pseudo time marching method to solve steady state cases. The pseudo time step size is equivalent to  $40.0^\circ$  of runner rotation. Unsteady simulations are initialized with the corresponding steady state simulation. Due to the large simulation domain many revolutions are necessary to reach convergence and statistically valid results. To speed up this process the initial time step size is set to  $\Delta t \hat{=} 40.0^\circ$  runner rotation per time step. After 30 revolutions the time step size is ramped down linearly over 100 iterations to the final time step size of  $\Delta t \hat{=} 5.0^\circ$  runner rotation. After a total build up time of about 42 revolutions time averaging is started. Eventually, the data is averaged over a period of 22 revolutions.

### B. Mesh generation and mesh study

Meshing is done with ICEM CFD in version 19.2. A hybrid mesh is used for the double turbine configuration. As shown in Fig. 3 the outer part of the farfield, the boundary layer of the dynamometers and the turbine domains are meshed with a block structured hexahedral mesh. The near field around the turbines is meshed with an unstructured tetrahedral mesh. A transition layer of pyramids connects the tetrahedrons to the hexahedrons. Prism layers with 20 elements normal to the wall are used to capture the boundary layer at the spherical ends of the hub near the blades. The unstructured mesh in the interaction zone of the turbines ensures a similar mesh quality and resolution independent of the radial distance between the turbines. Furthermore, this approach allows for an easier meshing process. For the most part the dimensionless wall distance  $y^+$  is smaller than 1 with few localized maximum values of 3 in all domains. A growth rate of element size normal to the walls between 1.2 and 1.3 ensures a proper resolution of the boundary layer.

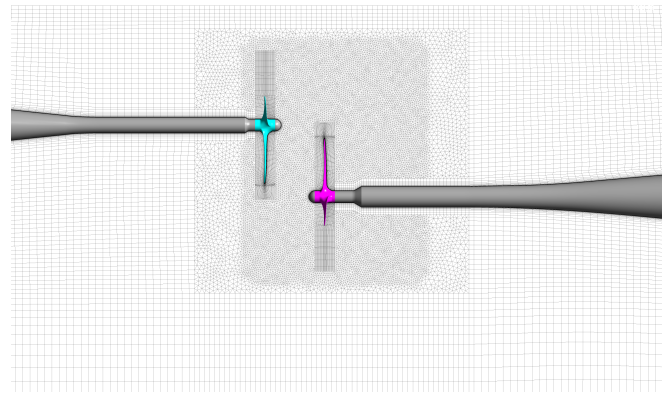


Fig. 3. Final hybrid mesh in double turbine configuration for a radial distance  $r/D_d = 0.6$ . Block structured hexahedral mesh around the dynamometers and in the farfield and turbine domains. Unstructured tetra dominant mesh in the near field around the turbines.

In the single turbine configuration a block structured mesh is used solely. The number of elements and the block structure of the turbine domain is the same as in the double turbine configuration. The normal wall distance of the first elements is adapted to reach a similar  $y^+$  value. The block structure of the far field differs due to the interface to the cylindrical turbine domain. Nevertheless, the overall distribution of elements and resolution of the boundary layer is quite similar. Furthermore, for this case a second mesh with an average value of  $y^+$  of about 60 is generated to estimate the influence of the treatment of the boundary layer.

For both configurations the element size and distribution of the turbine domain and the farfield domain including the dynamometers is adopted from previous investigations of the original size SIT250 turbine and its mounting to the PLAT-I platform. For the unstructured near field between the turbines an additional mesh study with three different meshes for a radial distance of  $r/D_d = 0$  was conducted. For each mesh a steady state simulation was performed. In contrast to all other steady state simulations a frozen rotor interface is used to connect the domains instead of a mixing plane interface. In a frozen rotor interface the variables are transferred directly at the interface and are only interpolated to the non-conformal meshes. Because of that the simulation results are dependent on the relative position of the domains, e.g. the relative position of the blades of the turbines to each other or the dynamometers. On the other hand this allows to account for some interaction between the domains and the frozen rotor approach should lead to bigger differences between the meshes compared to a mixing plane interface.

Apart from the near field around the turbines, all three meshes are the same. Compared to the mesh in Fig. 3 used ultimately the two additional meshes in Fig. 4 have a smaller refinement area around the two turbines. The finer mesh on the left side has half the element size and the mesh on the right the same element size in this refinement area as the final mesh. There is virtually no difference in the power and thrust

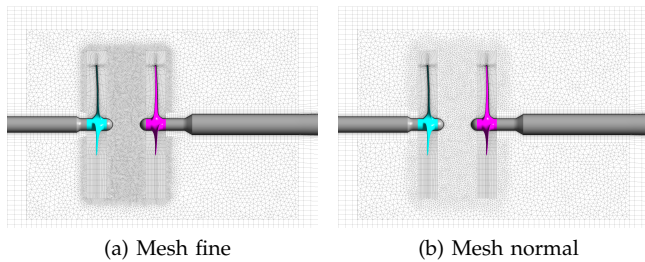


Fig. 4. Additional meshes for mesh study of near field with smaller refinement area around the turbines.

coefficient of both turbines between the final mesh and the normal mesh. Compared to the finer mesh the maximum absolute differences are  $\Delta C_P = 0.001$  and  $\Delta C_T = 0.0016$ . When comparing the different meshes visually, the longer refinement area downstream the second turbine allows for a more detailed resolution of the wake of the second turbine and intermixture with the outflow of the first turbine.

In the final mesh a  $120^\circ$  degree segment of a turbine containing one blade consist of about  $0.6 \cdot 10^6$  nodes or elements. The farfield size varies depending on the investigated geometry between  $4.2 \cdot 10^6$  and  $6.5 \cdot 10^6$  nodes. Due to the unstructured part of the mesh this is equivalent to  $7.0 \cdot 10^6$  to  $13.3 \cdot 10^6$  elements. The total mesh size of the whole simulation domain adds up to  $7.7 \cdot 10^6$  to  $10.0 \cdot 10^6$  nodes or  $10.3 \cdot 10^6$  to  $16.6 \cdot 10^6$  elements.

## V. SIMULATION RESULTS OF SINGLE TURBINE CONFIGURATION

The single turbine configuration is simulated to validate the numerical setup and to examine the accuracy compared to the experimental study. Fig. 5 shows the thrust coefficient  $C_T$  and power coefficient  $C_P$  at a freestream velocity  $u_\infty = 3$  m/s and different tip speed ratios  $\lambda$  for the experiment (exp) and two unsteady simulations. The first simulation (sim) has an average  $y^+$  of about 60 and utilizes wall functions for the boundary layer. The second simulation (sim  $y^+=1$ ) utilizes a mesh with an average  $y^+$  smaller than 1 and direct calculation of the boundary layer.

Initial calculations were performed for the rated tip speed ratio  $\lambda = 5$ . Resolving the boundary layer leads to a better agreement in both thrust and power. A possible explanation of the differences between the two simulations is a laminar turbulent transition of the boundary layer. The lower critical Reynolds number denotes the flow condition, where the transition from laminar to turbulent boundary layer occurs for the first time. For wings and blades the transition starts near the trailing edge. With increasing Reynolds number the transition point advances to the leading edge until the entire boundary layer is turbulent. The specific critical Reynolds number depends on the investigated geometry and is in the region of  $Re_{crit} \in [1.0 \cdot 10^3, 2.0 \cdot 10^5]$  for wings and blades [13]–[15]. The Reynolds number of the turbine calculated with the relative velocity and chord length at 70% radius is  $Re_{70} = 5.3 \cdot 10^5$ . Therefore

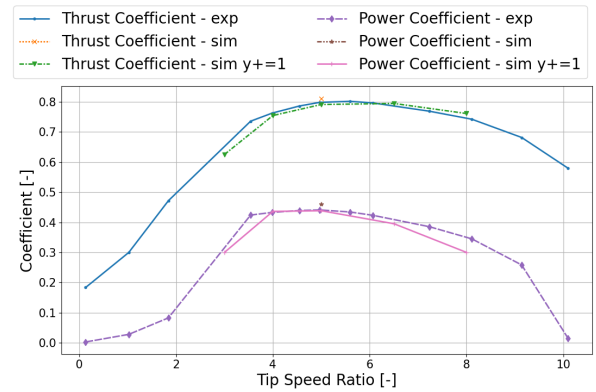


Fig. 5. Power and thrust coefficient for single turbine configuration. exp: experimental data. sim: simulation with wall function for boundary layer. sim  $y^+=1$ : simulation with resolved boundary layer.

it is possible that in the experiment the transition to a fully turbulent boundary layer is not yet finished and that at least parts of the boundary layer are still laminar. As common in standard RANS simulations the used models for the turbulence and boundary layer can not correctly predict the laminar turbulent transition of the boundary layer in general. Nonetheless a resolved boundary layer is a more accurate representation of the actual conditions and can lead to better results.

Because of that the characteristic curve was only simulated for the setup with resolved boundary layer. The overall agreement between experimental and simulated data is quite good. This is especially true near the rated tip speed ratio, whereas the accuracy decreases at the upper and lower limit. For higher tip speed ratios the thrust is overpredicted and for lower tip speed ratios underpredicted. The power exhibits a opposite behaviour. Due to the results of this investigation all simulations of the double turbine configuration are performed with a mesh capable of resolving the boundary layer.

## VI. EXPERIMENTAL AND SIMULATION RESULTS OF DOUBLE TURBINE CONFIGURATION

### A. Experimental results

Thrust coefficients  $C_T$  and torque coefficients  $C_Q$  measured in the experiment at a freestream velocity  $u_\infty = 1.5$  m/s for three different tip speed ratios  $\lambda = [3.0, 4.0, 5.0]$  are shown in Fig. 6. The coefficients are normalized with the mean of all cases  $r/D \in [1.2, 2.0]$ . Independent of  $\lambda$  a mutual influence of the turbines is detectable up to a radial distance of  $1D$ . Fluctuations of the measured values for higher radial distances correspond to the measuring accuracies of the used dynamometers. As expected the second turbine is much more influenced. The bulk of data of the first turbine exhibits a similar trend regardless of the tip speed ratio. Both thrust and torque of the second turbine decrease with increasing  $\lambda$ . This is probably an effect of the second turbine working in increasing off-design conditions.

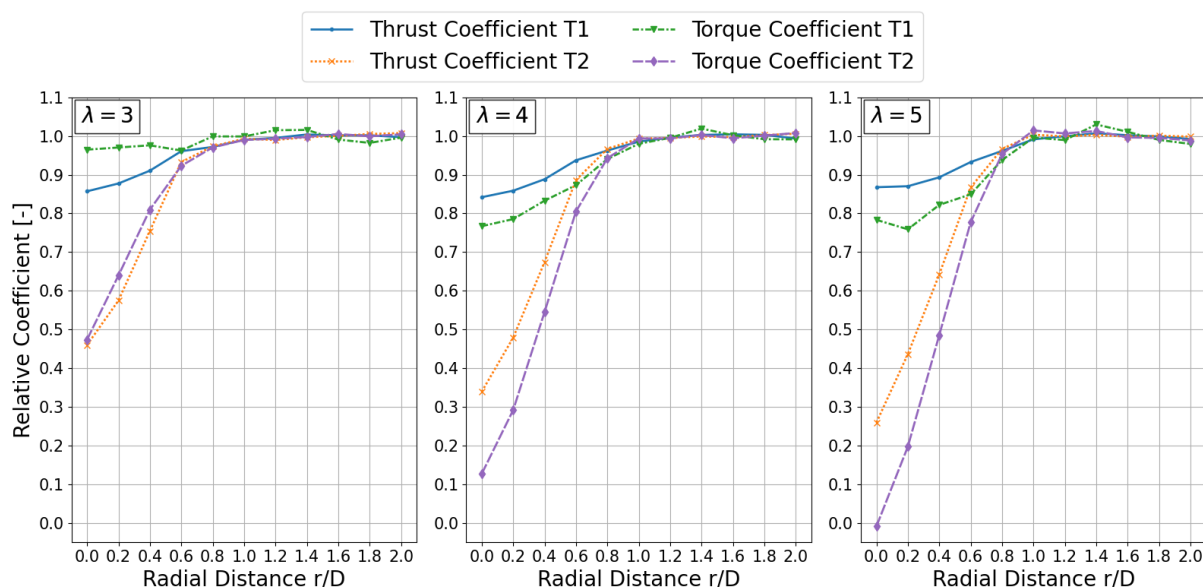


Fig. 6. Measured coefficients normalized with the mean of the cases  $r/D \in [1.2, 2.0]$ . T1: upstream turbine. T2: downstream turbine.

### B. Comparison of experimental and simulation results

Fig. 7 shows the absolute thrust and torque coefficients for different radial distances and both turbines (T1, T2) of the experiment (exp), the steady state simulation with mixing plane interface (steady MP) and the unsteady simulation (unsteady). In all cases the tip speed ratio  $\lambda$  is 4. Equally to the experimental data an interaction between the turbines is only visible up to a radial distance of  $r = 1.0D_d$  in the simulations. The general trend is captured by both simulations. In the experiment both thrust and torque of both turbines are quite similar for higher radial distances, whereas a difference in the simulation results is visible. At least partly these differences can be explained with the wake and boundary layer of the first dynamometer entering the upstream turbine as visible in Figs. 14a and 14c, whereas the second turbine has an undisturbed inflow. The wake recovery in standard RANS simulations tends to be underestimated, leading to a possible overestimation of the influence of the upstream dynamometer on the first turbine.

In most of the simulations the thrust is overestimated compared to the measurements. Furthermore there is a more or less constant offset for the first turbine and for higher radial distances in the second turbine between the simulations and experiment. Similar to section V a possible explanation for that is a laminar boundary layer in the experiment. Due to the lower diameter and inflow velocity the Reynolds number for this setup is only  $Re_{70} = 1.0 \cdot 10^5$ , which is in range of the critical Reynolds number reported in literature. Compared to a turbulent boundary layer the velocity gradient normal to the wall in a laminar boundary layer is lower. This leads to lower wall shear stresses and in consequence to a lower thrust. A significant deviation of the characteristic curves for the turbines at high radial distances compared to model tests at supercritical Reynolds numbers (not shown in this paper) and the better agreement of thrust coefficients of

the downstream turbine T2 for lower radial distances, where a turbulent boundary in the experiment is more likely due to interactions with the outflow of the first turbine, support this assumption.

Within the simulations there is an almost constant offset of thrust and torque for the first turbine and for higher radial distances in the second turbine. A systematic error between the simulations is assumed, because of the consistency of the error. This systematic error is probably an effect of the positioning of the interfaces between the rotating turbine domains and the farfield domain. If there is an uniform inflow and no unsteady effects, which is the case for the second turbine at higher radial distances, only minor or no differences at all are expected between a mixing plane and a transient rotor stator interface, if the distance of the interface to the blades is big enough. Due to the small distance in axial direction between the turbines, the interfaces of the turbine domains are in close proximity to the turbine blades. This close proximity in combination with the averaging of variables in circumferential direction in the mixing plane interfaces affects the flow in the near region of the blade, which can be seen in Fig. 9.

In Fig. 8 thrust and torque coefficients normalized with the results of the case  $r/D = 1.2$  are shown. Although there are differences in the absolute values in the simulations and measurements the relative effect of the interference on the performance of the turbines is quite similar for all cases.

### C. Analysis of unsteady simulation results

Figs. 10a and 10b show the phase averaged torque coefficient normalized with the mean of the simulation  $r/D = 1.2$  for the first and second turbine, respectively. The thrust coefficients exhibit a qualitative similar behaviour and are not shown. To get phase averaged values the regarded variable is time averaged for a fixed position of the turbine. In the present simulations

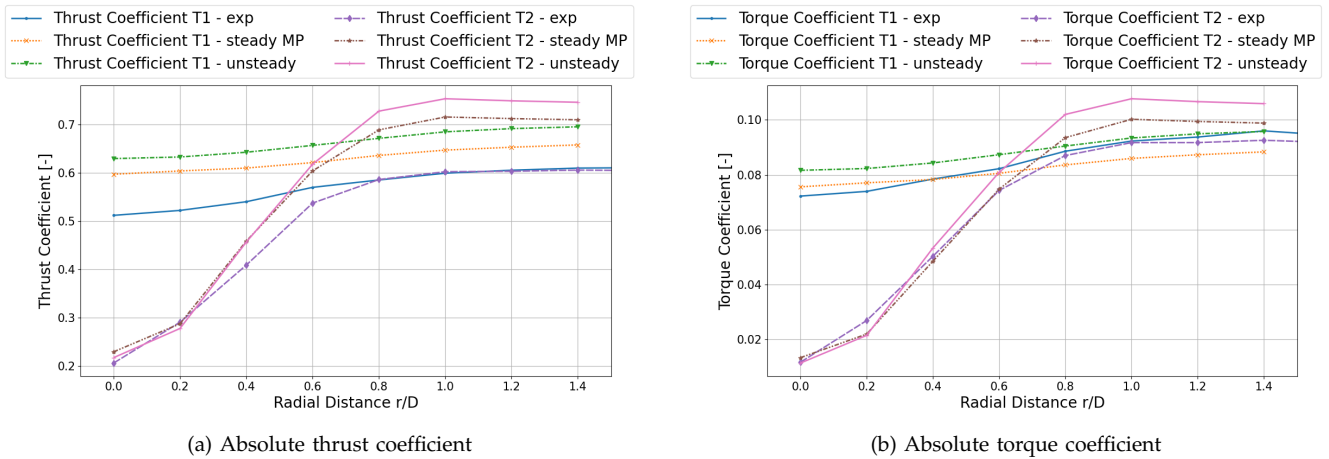


Fig. 7. Absolute thrust and torque coefficient of experiment and simulations. T1: upstream turbine. T2: downstream turbine. exp: experimental data. steady MP: steady state simulation with mixing plane interface. unsteady: unsteady simulation.

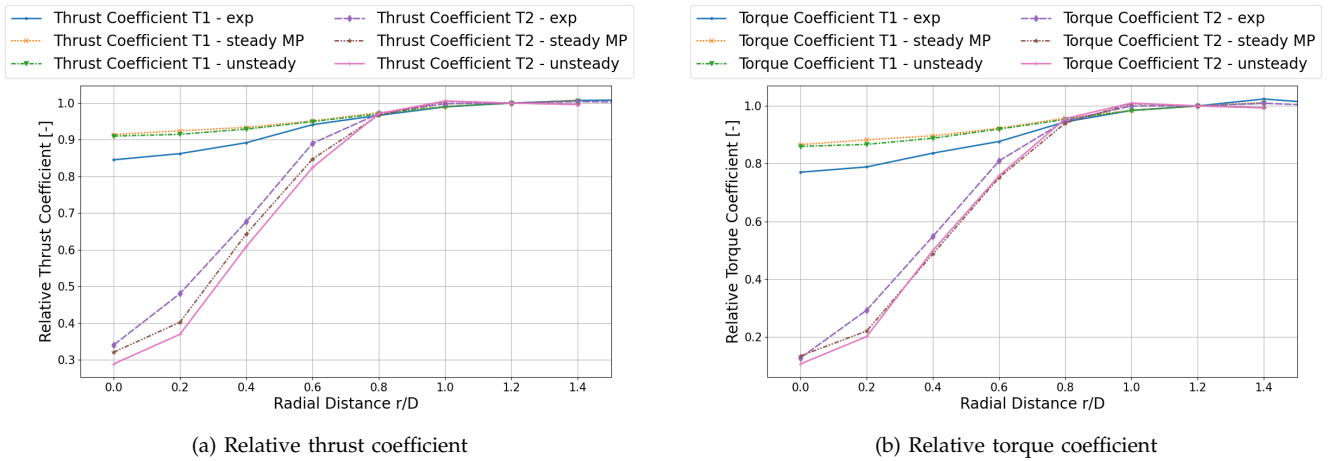


Fig. 8. Relative thrust and torque coefficient of experiment and simulations. Coefficients relative to results of case  $r/D = 1.2$ . T1: upstream turbine. T2: downstream turbine. exp: experimental data. steady MP: steady state simulation with mixing plane interface. unsteady: unsteady simulation.

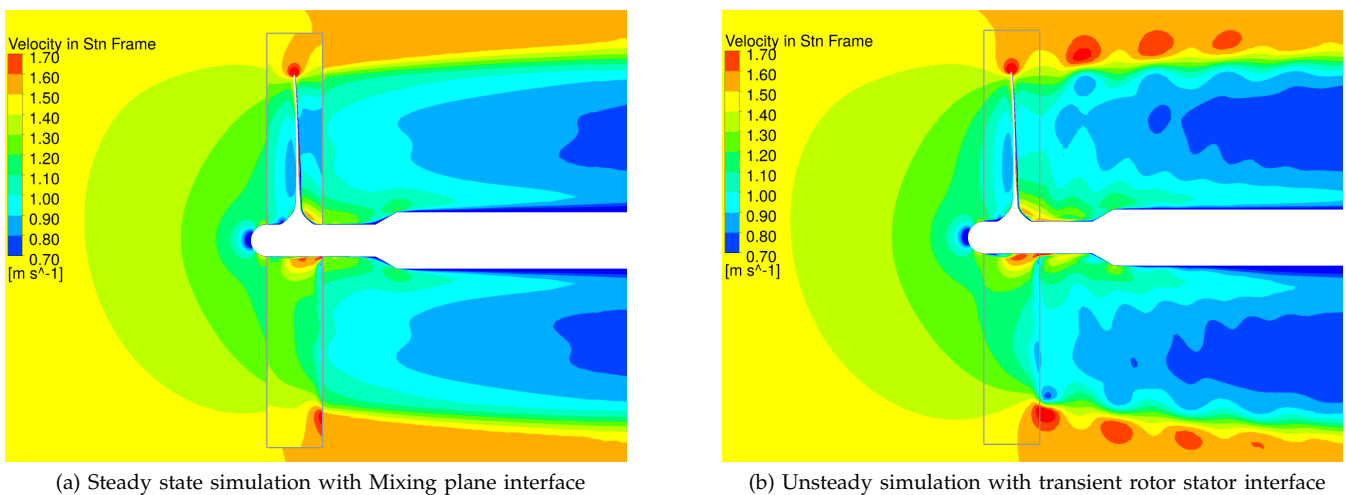
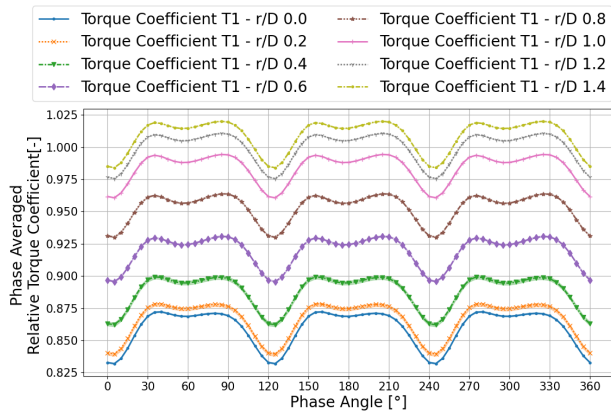


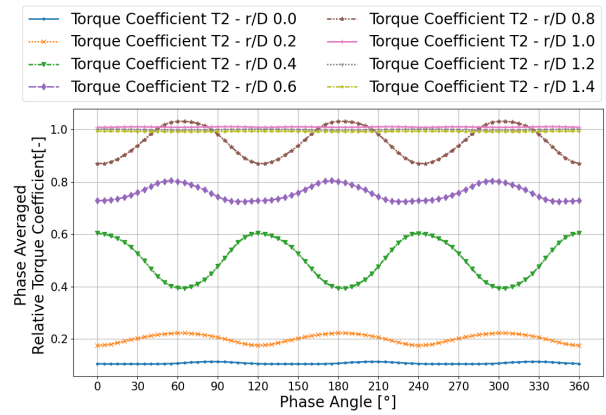
Fig. 9. Contour plot of absolute velocity in stationary frame around the second turbine. Interfaces depicted as grey lines. Simulation  $r/D = 1.4$ .

this leads to 72 data points each averaged over 22 revolutions due to the time step size of  $\Delta t \hat{=} 5.0^\circ$  and the time averaging period of 22 revolutions. A phase angle of  $\Phi \in [0^\circ, 120^\circ, 240^\circ]$  denotes that one of the three blades of the turbine is vertical and in top

position. The minimum and maximum value for each phase angle  $\Phi$  are shown as translucent shades around the mean. In both figures the extreme values are barely visible for all cases. This means, that there are no significant unsteady effects. The results are quasi-



(a) Upstream turbine T1



(b) Downstream turbine T2

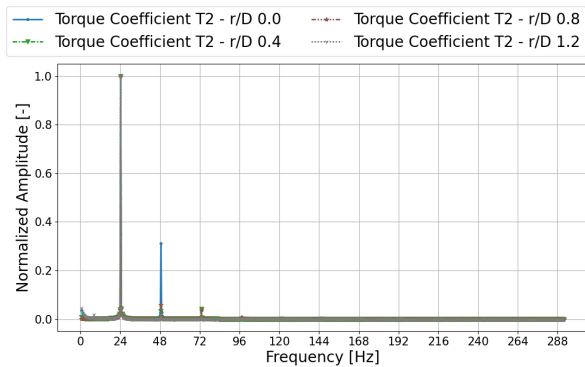
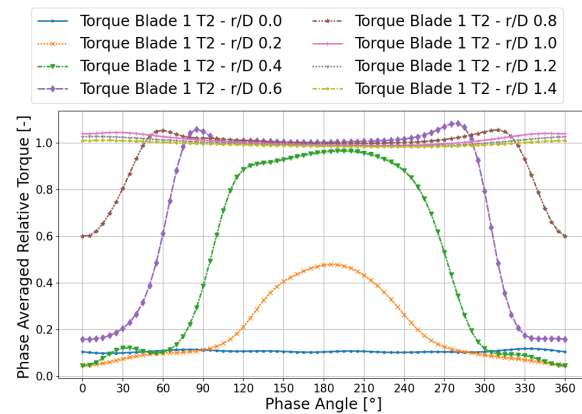
 Fig. 10. Phase averaged torque coefficients for both turbines relative to mean of case  $r/D = 1.2$ . A phase angle  $\Phi \in [0^\circ, 120^\circ, 240^\circ]$  denotes one blade of the turbine being in top vertical position.


Fig. 11. Fast Fourier Transformation of torque coefficient of second turbine for every second simulation. Blade passing frequency of 24.4 Hz.


 Fig. 12. Phase averaged torque of blade 1 of second turbine. Torque relative to average torque of case  $r/D = 1.2$ . A phase angle  $\Phi = 0^\circ$  denotes the blade being in top vertical position.

steady with respect to the phase and only dependent on the rotational position. The sole dependency on rotational position can also be seen in Fig. 11, where a Fast Fourier Transformation of the torque coefficient of the second turbine is shown. The only significant amplitudes occur for the blade passing frequency of about 24.4 Hz and multiples of that.

The trend of the torque coefficient of the first turbine in Fig. 10a is virtually the same for all radial distances and only shifted by a constant offset. The three minimum values correlate with either one of the blades being in top vertical position and in the the wake of the dynamometer. Only for radial distances between 0.2 and 0.8 the trends of the second turbine in Fig. 10b exhibit a distinct dependency on the phase. In these cases the oscillation is not an effect of the wake, but rather of the first turbine. Depending on the rotational position the blades of the second turbine are in the outflow of the first turbine or in the undisturbed flow underneath.

For a more detailed analysis the phase averaged torque for one blade of the second turbine is shown in Fig. 12 and the corresponding relative position and inflow to the turbine for  $r/D = 0.4$  and  $r/D = 0.8$

is presented in Fig. 13. For a phase angle  $\Phi = 0^\circ$  the blade is in top vertical position. The cases  $r/D = 0.4$  and  $r/D = 0.6$  exhibit the highest oscillations. For those cases during the course of one revolution the blade changes its location from being almost completely inside the outflow of the first turbine to being almost completely in the undisturbed flow and back. This leads to high differences in the flow conditions depending on the relative position, whereas the other cases experience a more uniform inflow in the form of either the disturbed outflow or the undisturbed flow most of the time. The change of flow conditions shown in Fig. 13 matches perfectly with the trend of torque. The vorticity as a measure of the turbulent structures shows the three tip vortices and the hub vortex. The tip vortices correspond with the high velocities and rotate the same way, whereas the hub vortex is basically static in the shown plane. Both the velocity and vorticity display the limited area, where an influence of the first turbine is present.

This limited influence is also observed in Fig. 14, where the absolute velocity in a side view (left side) and an isosurface of the velocity invariant  $Q$  as a representation of the vortices (right side) are displayed

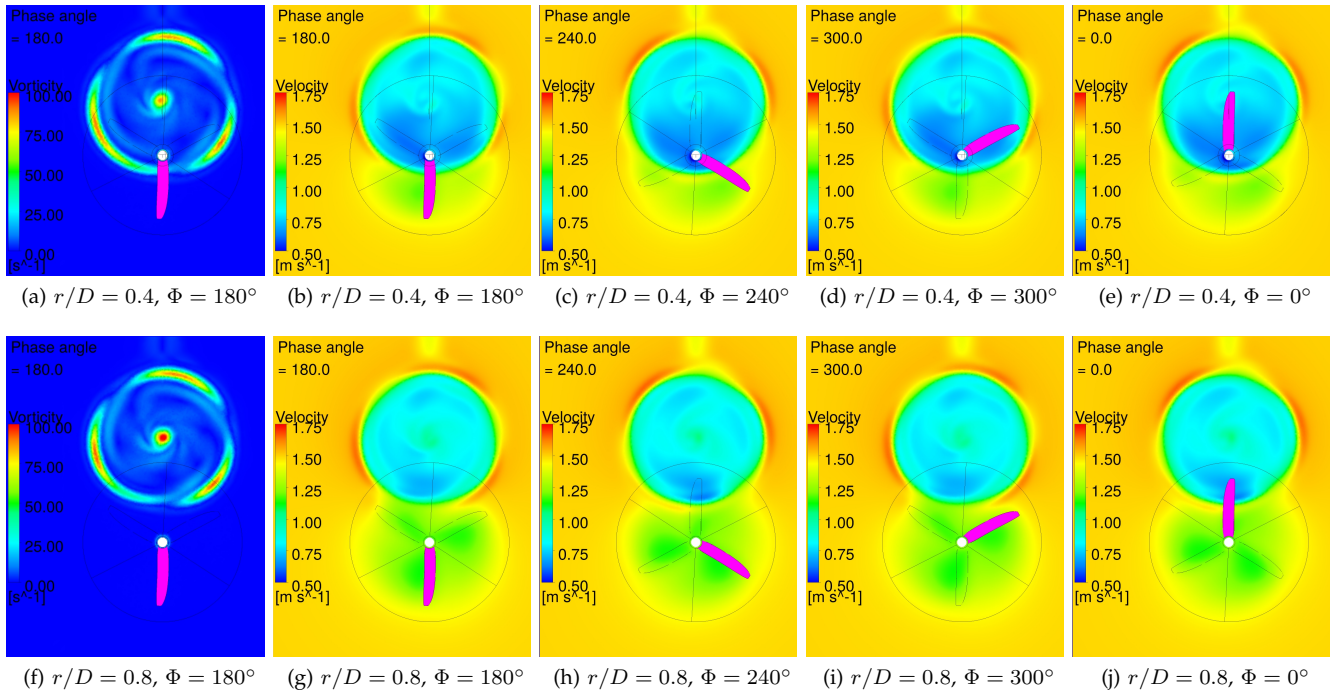


Fig. 13. Instantaneous vorticity and velocity in a plane shortly upstream of turbine T2. Blade 1 (cf. Fig. 12) shown in magenta. Results of simulations  $r/D = 0.4$  and  $r/D = 0.8$  for different phase angles  $\Phi$ . Direction of view against flow direction. First turbine (not visible) rotating clockwise, second turbine rotating counterclockwise.

for radial distances of  $r/D = 0.4$  and  $r/D = 1.2$ . For the first turbine one blade is in bottom vertical positions ( $\Phi = 180^\circ$ ) and for the second turbine one blade is in top vertical position ( $\Phi = 0^\circ$ ). Downstream the first turbine the flow velocity is reduced from  $u_\infty = 1.5$  m/s to about 0.9 m/s. In the case of an overlapping of the turbine blades the velocity between the turbines is further reduced. Both observations are also made in Fig. 13. The tip vortices are visible as areas of high velocity. In the case  $r/D = 0.4$  the tip vortices of the first turbine interact with the hub of the second turbine. Furthermore, the hub vortex of the first turbine and the tip vortices of the second turbine mix and suppress the normal development of the tip vortices. These interactions between the vortices lead to large areas with very low velocities. For the case  $r/D = 1.2$  the turbines interact only in a small area between them, where the stream tubes downstream of the turbines are shifted upwards for the first turbine and downwards for the second turbine respectively.

## VII. CONCLUSION

Simulations and measurements for a single turbine and a double turbine configuration in model scale have been shown and compared. Due to the small diameter of the investigated turbines, at least parts of the boundary layer are suspected to be laminar. This is especially true for the double turbine configuration with even smaller diameters than the single turbine.

The single turbine was investigated at different tip speed ratios  $\lambda$ . Resolving the boundary layer with a mesh with  $y^+ < 1$  instead of using wall functions leads to a better and overall good agreement of the simulation results with the experiment. Due to these results

the same simulation approach and a comparable mesh have been used for the double turbine configuration.

In the double turbine configuration the turbines are arranged one after another with a fixed axial distance  $a = 0.5D_d$  and a variable radial distance of  $r \in [0.0D_d, 2.0D_d]$ . The results of measurements for three different tip speed ratios  $\lambda$  and steady state and unsteady simulations for one  $\lambda$  are shown. In both the experiments and simulations a mutual interference between the turbines is only visible up to a radial distance of about one diameter  $a/D_d = 1.0$ . In the experimental results the relative performance of the second turbine decreases with increasing tip speed ratio. The general trend of thrust and torque coefficient for both turbines is captured by both simulation approaches. Nonetheless there are small differences in the absolute values in between the simulations and compared to the experiment. A possible explanation for the deviation to the experiment is a laminar turbulent transition of the boundary layer in the experiment, which can not be captured accurately by the employed simulation approach. Due to geometric restrictions the interfaces between the rotating turbine domains and the static farfield are in close proximity to the turbine blades, possibly leading to the differences between the steady state and unsteady simulation for higher radial distances. When looking at the relative influence on the performance of the turbine compared to the undisturbed values, the results of the experiment and simulations are quite similar. In the unsteady simulations it is seen, that the interaction between the turbines is only dependent on the phase (relative position) of the blades and no unsteady effects can be detected. All in all the simulations can predict the interaction and behaviour of the turbines quite accurately. If the only

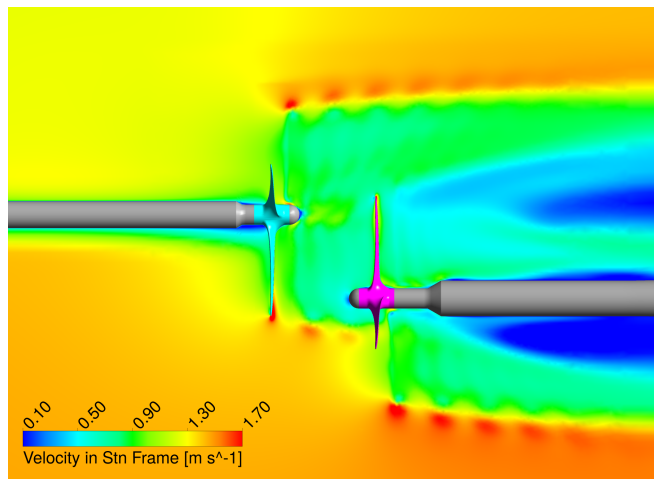
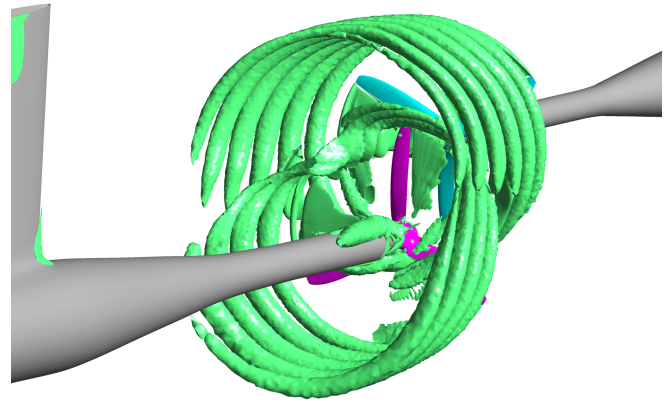
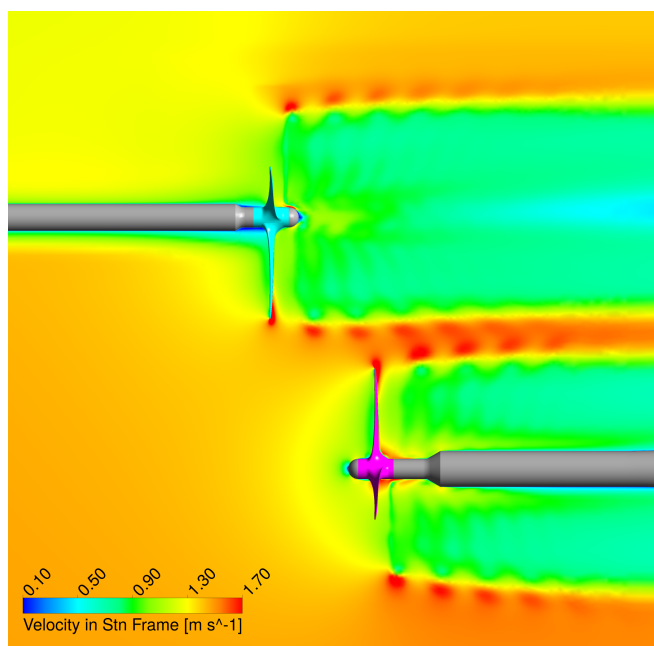
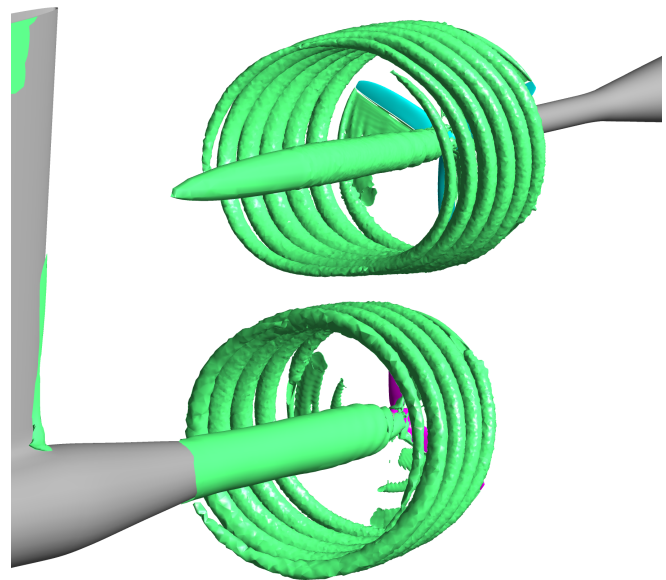

 (a) Absolute velocity in stationary frame,  $r/D = 0.4$ 

 (b) Isosurface of velocity invariant  $Q$ ,  $r/D = 0.4$ 

 (c) Absolute velocity in stationary frame,  $r/D = 1.2$ 

 (d) Isosurface of velocity invariant  $Q$ ,  $r/D = 1.2$ 

 Fig. 14. Simulations for  $r/D = 0.4$  and  $r/D = 1.2$ . Left: Instantaneous absolute velocity in stationary frame. Right: Isosurface of velocity invariant  $Q$  to visualize vortices.

interest is in the relative influence on the performance of the turbines a steady state simulation is sufficient, whereas a detailed analysis is only possible with an unsteady simulation.

For future work simulations with a transition prediction model for the boundary layer might be of interest to investigate if the agreement between measurements and simulations can be improved by that. Furthermore, simulations of the double turbine configuration with the additional tip speed ratios used in the experiment would allow to investigate the different impact on the second turbine. Finally investigations with a variable tip speed ratio for the second turbine adapted to the inflow conditions resulting from the first turbine would be interesting to examine to what extend or whether at all the interference of the turbines can be influenced and reduced.

## REFERENCES

- [1] R. Starzmann, I. Goebel, and P. Jeffcoate, "Field performance testing of a floating tidal energy platform-part 1: Power performance," in *Proc. of the 4th AWTEC*, Taipei, Taiwan, 2018.
- [2] R. Starzmann, N. Kaufmann, and P. Jeffcoate, "Full and model scale testing of two different rotor diameters for in-stream power generation," in *Proc. of the 13th EWTEC*, Napoli, Italy, 2019.
- [3] N. Kaufmann, T. H. Carolus, and R. Starzmann, "Turbines for modular tidal current energy converters," *Renewable Energy*, vol. 142, pp. 451–460, 2019. [Online]. Available: <https://www.sciencedirect.com/science/article/pii/S0960148119306044>
- [4] L. E. Myers and A. S. Bahaj, "An experimental investigation simulating flow effects in first generation marine current energy converter arrays," *Renewable Energy*, vol. 37, no. 1, pp. 28–36, 2012. [Online]. Available: <https://www.sciencedirect.com/science/article/pii/S0960148111001716>
- [5] T. Stallard, R. Collings, T. Feng, and J. Whelan, "Interactions between tidal turbine wakes: experimental study of a group of three-bladed rotors," *Phil Trans R Soc A 371: 20120159*, 2013.
- [6] P. Mycek, B. Gaurier, G. Germain, G. Pinon, and E. Rivoalen, "Numerical and experimental study of the interaction between two marine current turbines," *International Journal of Marine Energy*, vol. 1, pp. 70–83, 2013. [Online]. Available: <https://www.sciencedirect.com/science/article/pii/S2214166913000088>

- [7] P. Mycek, B. Gaurier, G. Germain, G. Pinon, and E. Rivoalen, "Experimental study of the turbulence intensity effects on marine current turbines behaviour. Part II: Two interacting turbines," *Renewable Energy*, vol. 68, pp. 876–892, 2014. [Online]. Available: <https://www.sciencedirect.com/science/article/pii/S0960148114000196>
- [8] R. Malki, I. Masters, A. J. Williams, and T. Nick Croft, "Planning tidal stream turbine array layouts using a coupled blade element momentum – computational fluid dynamics model," *Renewable Energy*, vol. 63, pp. 46–54, 2014. [Online]. Available: <https://www.sciencedirect.com/science/article/pii/S0960148113004412>
- [9] W. Hunter, T. Nishino, and R. H. J. Willden, "Investigation of tidal turbine array tuning using 3d reynolds-averaged navier–stokes simulations," *International Journal of Marine Energy*, vol. 10, pp. 39–51, 2015. [Online]. Available: <https://www.sciencedirect.com/science/article/pii/S221416691500003X>
- [10] A. Olczak, T. Stallard, T. Feng, and P. K. Stansby, "Comparison of a rans blade element model for tidal turbine arrays with laboratory scale measurements of wake velocity and rotor thrust," *Journal of Fluids and Structures*, vol. 64, pp. 87–106, 2016. [Online]. Available: <https://www.sciencedirect.com/science/article/pii/S088997461530058X>
- [11] N. Kaufmann, T. H. Carolus, and R. Starzmann, "An enhanced and validated performance and cavitation prediction model for horizontal axis tidal turbines," *International Journal of Marine Energy*, vol. 19, pp. 145–163, 2017. [Online]. Available: <https://www.sciencedirect.com/science/article/pii/S2214166917300589>
- [12] Quality Systems Group of the 28th ITTC, "ITTC - recommended procedures and guidelines - open water test," ITTC, Tech. Rep. 7.5-02-03-02.1 Rev. 03, 2014. [Online]. Available: <http://www.ittc.info/media/8025/75-02-03-021.pdf>
- [13] B. H. Carmichael, "Low Reynolds Number airfoil survey," NASA, Tech. Rep. Report No. 165803, 1981.
- [14] K. Yousefi and A. Razeghi, "Determination of the critical reynolds number for flow over symmetric naca airfoils," in *2018 AIAA Aerospace Sciences Meeting*. [Online]. Available: <https://arc.aiaa.org/doi/abs/10.2514/6.2018-0818>
- [15] W. Du, Y. Zhao, H. Liu, and Y. He, "Analysis of the critical reynolds number for floating wind turbine blades," in *Pacific/Asia Offshore Mechanics Symposium*, 2014, iSOPE-P-14-075.